Frequency-Dependent Pathloss in the Ultrawideband Indoor Channel

Wasim Q. Malik, David J. Edwards, and Christopher J. Stevens

Abstract— **The frequency-dependent pathloss characteristics of an indoor radio channel are investigated over the FCC-allocated ultrawideband (UWB) frequency range (3.1–10.6 GHz). Complex channel transfer functions are measured under a variety of propagation conditions. The dispersion index is introduced as a measure of the frequency-dependence pathloss and is estimated for each measured channel response. Its first order statistics exhibit significant deviation from the nominal value. The small-scale spatial analysis of the dispersion index reveals a periodic structure for vertically polarized channels. Fractional calculus is used to demonstrate the impact of this dispersion on system performance, and the consequent signal waveform distortion is evaluated.**

Index Terms— **Dispersion, frequency-selective fading, propagation channel, pulse distortion, ultrawideband (UWB).**

I. Introduction

Ultrawideband (UWB) communications systems span very large bandwidths, typically up to several gigahertz [1]. As this signal bandwidth exceeds the indoor channel coherence bandwidth by many orders of magnitude [2], the frequency response of the channel is not flat, and the channel is said to be frequency-selective. Many system design aspects that are usually ignored in narrowband communications become quite significant in UWB systems. Among those is the frequency dependence of the channel, antennas, amplifiers, filters, and other components. From a link budget perspective, this phenomenon manifests itself in UWB systems in the form of frequency-dependent pathloss (FDP), causing non-uniform signal attenuation across the band.

The dominant source of FDP in most situations is the antenna pair [3]. The effective aperture of a constant-gain antenna is a function of frequency [4]. Therefore, as identified in [5], the apparent pathloss of the channel is influenced by frequency, where the channel is considered to be inclusive of the antenna pair. This is true for a pair of isotropic radiators, or omni-directional antennas when the propagation is primarily in the azimuthal plane. Any departure from the ideal behavior of perfect omni-directional antennas can be attributed to one or more of the following physical aspects of propagation:

1. diffraction across blocking objects [6];
2. scattering from textured surfaces [7];
3. wall penetration, with the material reflection coefficients being frequency-dependent [8, 9];
4. frequency-selective reflection from metallic objects of specific geometric shapes such as railings and gratings;
5. vector superposition of overlapping signal waveforms in a dense multipath channel, altering the frequency content of individual multipaths [10]; and
6. angular-spectral distortion of UWB antennas, resulting in significantly altered radiation characteristics [3].

As the indoor UWB channel experiences rich multipath propagation [11], there is a finite probability of significant FDP due to the aforementioned wave propagation and antenna distortion phenomena.

Non-uniform spectral behavior can severely degrade the performance of a communications receiver as shown in [12]. For this reason, it is important to characterize the extent of FDP so that the transmitter or receiver can compensate for it in an appropriate manner. This may involve pre-distortion filtering at the transmitter in a cognitive radio system [13], or frequency-domain automatic gain control at the receiver. Detailed discussion of these and other mitigation techniques will, however, be the subject of a future publication.

Acknowledging the significance of FDP, [14] modeled it with an exponential decay factor with mean values of 1.01 and 1.36 in line-of-sight (LOS) and non-line-of-sight (NLOS) environments, respectively. On the other hand, [15] used a power-law model and extracted the frequency transfer function amplitude decay exponent with 1 GHz frequency as reference. It reported exponents between 0.8 and 1.4 with variations by up to a factor of 2 over small distances in an office environment. A further refinement of this model, with the exclusion of antenna effects, led to exponents between -1.4 in industrial and 1.5 in residential environments [16].

The approach adopted in this paper is simpler and more natural as it relates directly to the propagation mechanism by estimating the frequency decay constant of the power spectrum. The proposed FDP model has the same functional form as the conventional distance-dependent pathloss, allowing a convenient formulation for the composite, bivariate pathloss $PL(d, f)$, where d and f represent the distance and frequency, respectively. The extraction of the FDP model parameter is based on the measured channel transfer function between a single transmit and receive antenna pair. The

This work was supported by the Engineering and Physical Sciences Research Council, U.K., under grant GR/T21769/01.

The authors are with the Department of Engineering Science, University of Oxford, Parks Road, Oxford OX1 3PJ, UK (e-mail: wasim.malik@eng.ox.ac.uk).

1-4244-0355-3/06/$20.00 (c) 2006 IEEE

This full text paper was peer reviewed at the direction of IEEE Communications Society subject matter experts for publication in the IEEE ICC 2006 proceedings.

probabilistic variation of the FDP index, henceforth referred to as the dispersion index and denoted by ξ, is characterized and its small-scale spatial variation is analyzed. In order to study the effect of polarization, the measured FDP with vertically and horizontally polarized antennas are compared.

II. Experimental Configuration

Frequency-domain UWB channel measurements were conducted in an indoor environment that consisted of a 6 m^2 laboratory with block walls, concrete floor and ceiling, a large glass window, and metallic and wooden furniture, as shown in Fig. 1. A vector network analyzer (VNA) arrangement was used to sound the channel at n_f = 1601 discrete frequencies in the UWB band [f_l, f_h] where f_l = 3.1 GHz and f_l = 10.6 GHz. The measurement bandwidth was thus B = 7.5 GHz and the resolution of the measurement was Δf = 4.7 MHz. Vector normalization was performed prior to measurement in order to remove the complex noise introduced by the equipment.

Discone antennas, linearly polarised and omni-directional in the azimuth plane, were used to conduct the measurement [3]. The location of the transmitting antenna was fixed, while the receiving antenna was hoisted on a positioning arm that scanned a 1 m^2 rectangular area in the form of a grid with a 0.01 m resolution. A computer was used for automatic data logging from the VNA via a GPIB link and also for controlling the location of the positioning arm on the measurement grid. Both line-of-sight (LOS) and non-line-of-sight (NLOS) propagation scenarios were considered. The latter was created by placing a large aluminum sheet between the transmitting antenna and the grid. The measurement was performed sequentially with the transmitting and receiving antennas polarizations vertically and horizontally. Thus a total of 40,000 UWB channel responses were recorded.

III. Dispersion Index Estimation

The narrowband Friis transmission equation describes the far-field propagation of an electromagnetic wave in freespace such that the pathloss is determined through the inverse square law [7]. With omni-directional antennas,

$$P_r = P_t G_t G_r \left(\frac{\lambda}{4\pi d} \right)^2 \tag{1}$$

where P_r and P_t are the received and transmitted powers, G_r and G_t are the receiving and transmitting antenna gains, d is the antenna separation, and λ is the of the signal wavelength. For a UWB system, the dependence on frequency, f, can be explicitly expressed as

$$P_r(f) = P_t(f) G_t(f) G_r(f) \left(\frac{c}{4\pi df} \right)^2, \tag{2}$$

where c = 3x10^8 m/s is the speed of light in freespace. Thus the freespace pathloss is nominally a quadratic function of frequency. In terms of the channel transfer function,

$$\left| H_{freespace}(f) \right| \propto f^{-\xi/2}, \qquad \xi = 2, \tag{3}$$

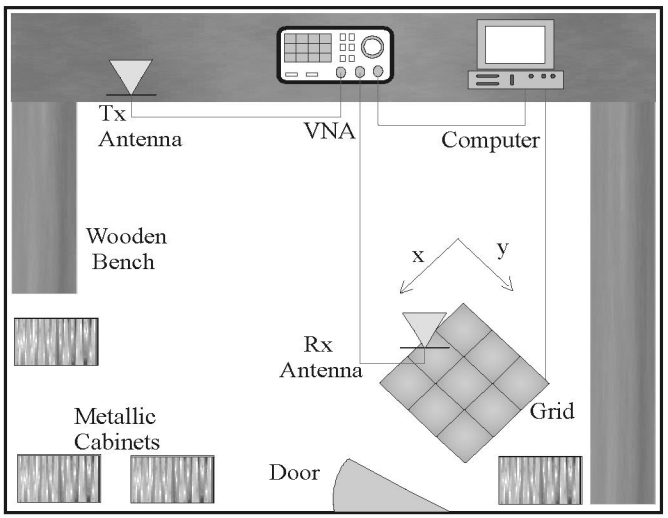

Fig. 1. A plan view of the measurement environment

where the pathloss exponent, ξ, that governs the dependence of the received power on frequency, has been introduced.

For a channel with spatio-temporal stationarity, ξ can be incorporated in (2) by assuming a constant antenna separation. Then the pathloss can be expressed in logarithmic scale explicitly as a function of ξ by

$$PL_{dB}(f) = 10\xi \log_{10} f + K, \tag{4}$$

where K is a constant. It is obvious from (4) that the logarithmic pathloss scales linearly with logarithmic frequency, which forms the basis of the model in this paper.

It is well known from antenna theory that ξ = 2 for constant-gain (omni-directional) antennas, which corresponds to a pathloss of 6 dB/decade. If constant aperture (directional) antennas are used at both ends, ξ = -2, while for one omni-directional and one directional antenna, ξ = 0. The regression of pathloss on frequency, in accordance with the preceding discussion, can be analyzed by plotting the pathloss derived from the measured power spectrum on a logarithmic frequency scale. The slope of the corresponding least-squares best-fit line provides an estimate of ξ. Fig. 2 shows a single measured transfer function along with the regression line.

IV. Dispersion Index Characterization

A. First Order Statistics

The dispersion index, ξ, is estimated for each frequency transfer function in the measured data using the above best-fit procedure. As our measurement uses omni-directional antennas, ξ is ideally expected to exhibit a value of 2. Fig. 3 shows the cumulative distribution functions (CDFs) of ξ for the four propagation cases under consideration, such that V_{LOS} represents the vertically polarized LOS channel, etc. It is observed that the median ξ is close to 2 only for V_{LOS}. The V_{NLOS} channel experiences slightly higher ξ, with median 2.1. Changing the polarization of the transmitting and receiving antennas, however, has a much more significant impact, so

This full text paper was peer reviewed at the direction of IEEE Communications Society subject matter experts for publication in the IEEE ICC 2006 proceedings.

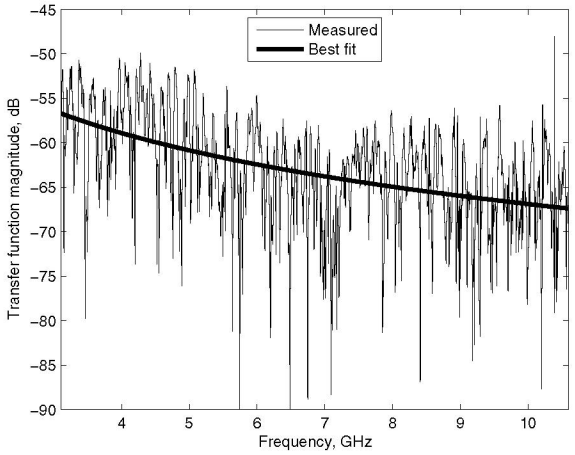

Fig. 2. A measured channel transfer function in the indoor LOS channel and its best-fit regression line from which the dispersion index is estimated

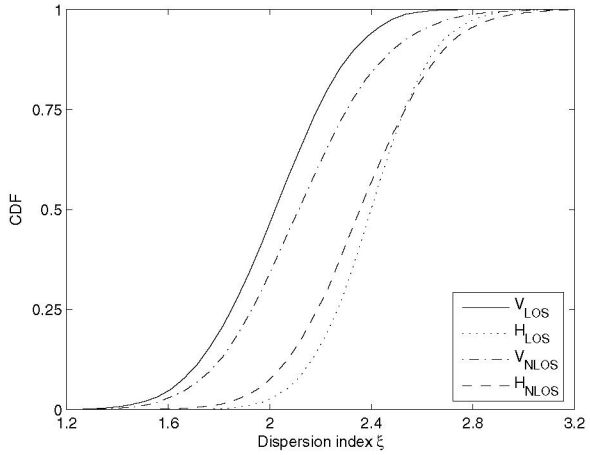

Fig. 3. The distribution of dispersion index obtained from channel measurements with horizontal and vertical polarizations

that the median ξ for H_{LOS} becomes 2.4. Similar to the vertically polarized link, the obstruction of LOS in the horizontal link does not have affect ξ drastically. In addition, a significant variance is observed in each case, as summarized in Table I.

From these observations, it can be inferred that the higher-end frequencies undergo greater attenuation in horizontally polarized channels than in vertically polarized channels. This points to the inherent polarization differences in the propagation mechanisms and environments.

B. Small-Scale Variation

Fig. 4 shows the variation of ξ in a 1 m^2 planar area in the form of intensity images. This representation indicates the values of ξ at the sequential measurement locations on the measurement grid in Fig. 1, and reconstructs the interference patterns of ξ in that region.

In accordance with the observations earlier in this paper, the vertical channels experience lower ξ compared to the horizontal channels measured at the same positions on the grid, in general. Distinct interference fringes are observed in Fig. 4 for the V_{LOS} channel. A deeper examination and comparison with Fig. 1 suggests that the pattern is closely related to the room geometry and is roughly aligned along the walls. The systematic spatial variation in dispersion index is thus related to the combination of dominant multipath arrivals from nearby reflecting objects.

The LOS and NLOS channels with a given polarization exhibit similar behavior in terms of the spatial variation of ξ, suggesting that the role of the direct path in determining this quantity is insignificant.

In the horizontally polarized channels, ξ is generally not only higher than in the vertically polarized channels, but also more uniform spatially, without the interference fringes observed for the vertically polarized channels. This observation suggests a tradeoff between the vertical and horizontal polarizations, as one offers a low but rapidly changing ξ while the other offers higher but more uniform ξ.

Also, the dispersion index for the horizontally polarized channel increases noticeably with distance. The observation of greater increase in horizontal pathloss with distance agrees with the results in [17], but further discussion of distance-dependent pathloss is beyond the scope of the current paper.

These observations prove that the deviation of ξ from its nominal, antenna-dependent value depends on the signal properties and the propagation environment. It is clear from the results that the dispersion index is not a constant quantity depending solely on the antennas. Thus, the current characterization disproves earlier works such as [5].

TABLE I
MEASURED DISPERSION INDEX STATISTICS

Environment	Polarization	Median	Std. Dev.
LOS	Vertical	2.04	0.24
LOS	Horizontal	2.42	0.20
NLOS	Vertical	2.15	0.28
NLOS	Horizontal	2.39	0.25

V. SIGNAL WAVEFORM DISTORTION

FDP affects the received signal, distorting its waveform. If $\xi > 0$, as is the case with an omni-directional antenna pair, the high frequency signal components are de-emphasized, altering its time-domain pulse-shape. From Fourier theory, therefore, a linear increase in pathloss with frequency f is in essence equivalent to integration, apart from phase rotation. To analyze the effect of this dispersion, assume that a signal $s(t)$ with Fourier transform $S(f)$ is distorted due to propagation through a channel with dispersion index ξ. The received signal is then given by

This full text paper was peer reviewed at the direction of IEEE Communications Society subject matter experts for publication in the IEEE ICC 2006 proceedings.

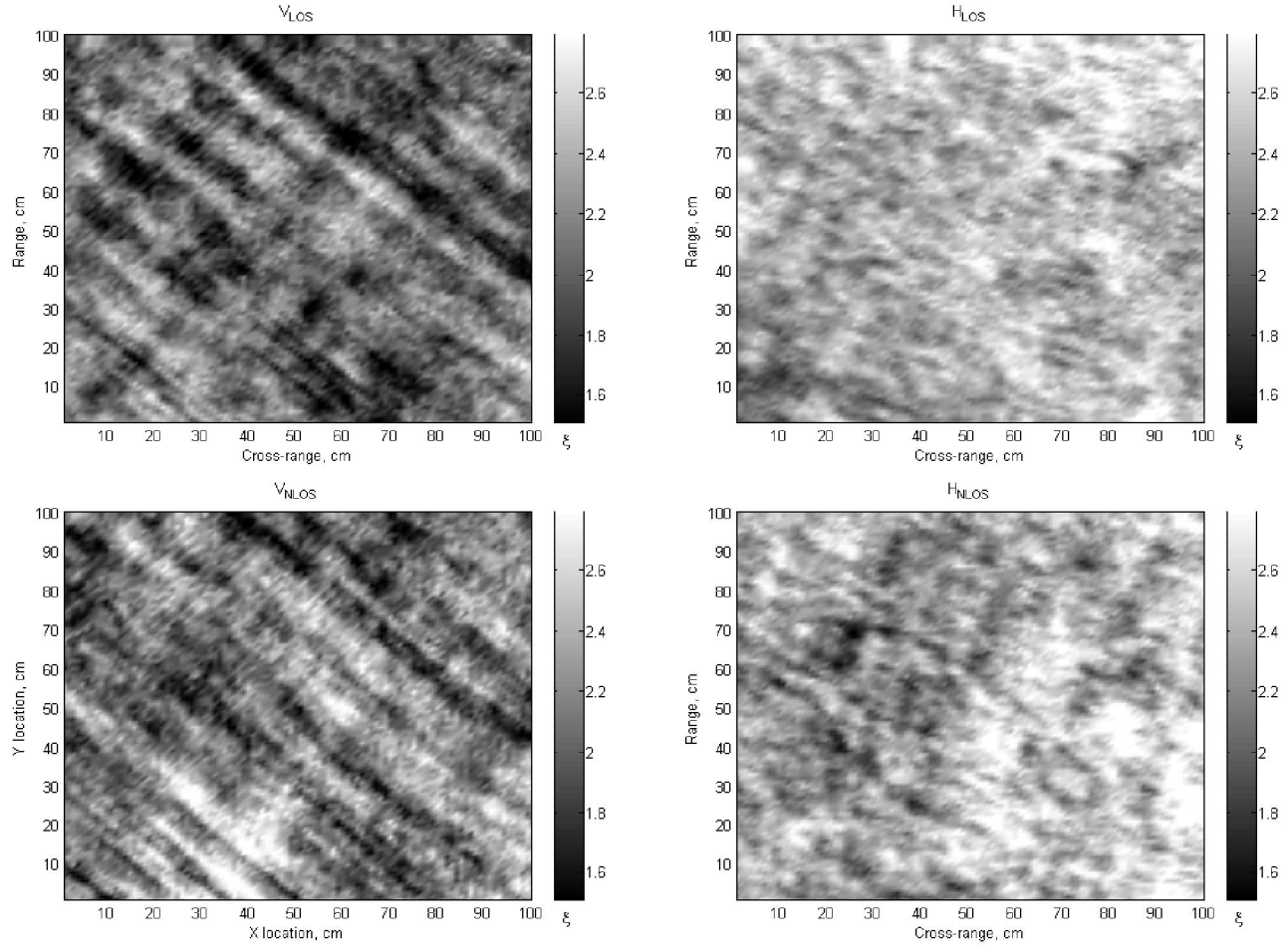

Fig. 4. Spatial variation of dispersion index, ξ, over a 1m^2 area. The lighter shades represent higher ξ, and the intensity images are normalized globally

$$r(t) = \mathcal{F}^{-1}\left[f^{-\nu}S(f)\right] = j2\pi D^{-\nu}s(t), \quad \forall\, \nu = \frac{\xi}{2} \geq 0, \quad (5)$$

where $\mathcal{F}^{-1}[.]$ denotes the inverse Fourier transform. The $D^{-\nu}$ operator in (5) denotes the ν-fold integral. As $\xi \in \mathcal{R}$, $D^{-\nu}$ represents the fractional integral given by [18]

$$D^{-\nu}x(t) = \frac{1}{\Gamma(\nu)}\int_0^t (t-\varsigma)^{\nu-1}\, x(\varsigma)\, d\varsigma, \quad (6)$$

with $\Gamma(\nu)$ denoting the gamma function.

If, on the other hand, $\xi < 0$, the fractional derivative of $s(t)$ is obtained instead [18].

In terms of waveform distortion, a conventional narrowband signal using a continuous-wave carrier only undergoes a phase variation as a consequence of such fractional calculus operations. A pulsed UWB signal, however, suffers from pulse-shape distortion due to FDP that changes the functional form of the signal.

The impact of this dispersion on a UWB communications system can be illustrated with the example of an impulse-based receiver [19]. A popular pulse waveform for such systems is the second derivative of Gaussian function. For the analysis here, it is assumed that this pulse, $s(t)$, provides the excitation to the transmitting antenna. To emphasize, the channel in this treatment is inclusive of the antennas, so that the overall signal dispersion due to the overall channel, comprising the two antennas and the wave propagation path between them, is characterised jointly.

Fig. 5 shows the response of dispersive UWB channels, with $\xi = \{-4,\ldots,4\}$, excited with the second derivative of Gaussian waveform. The effect of phase rotation is also illustrated by showing both the real and imaginary components. It can be observed that $\xi < 0$ transforms the original pulse waveform into higher order Gaussian pulses, an operation similar to time-domain differentiation, while $\xi > 0$ results in signal waveform integration. The pulse shape is preserved only for $\xi = 0$, where no dispersion takes place. Higher order Gaussian pulses have smaller relative bandwidths and higher centre frequencies. Thus FDP results in the translation and scaling of the signal spectrum. Also, the signal energy oscillates between the in-phase and quadrature states at the consecutive even values of ξ. It is complex at odd ξ with equal power distribution between the real and imaginary parts. For non-integer ξ, the signal assumes intermediate complex values.

This full text paper was peer reviewed at the direction of IEEE Communications Society subject matter experts for publication in the IEEE ICC 2006 proceedings.

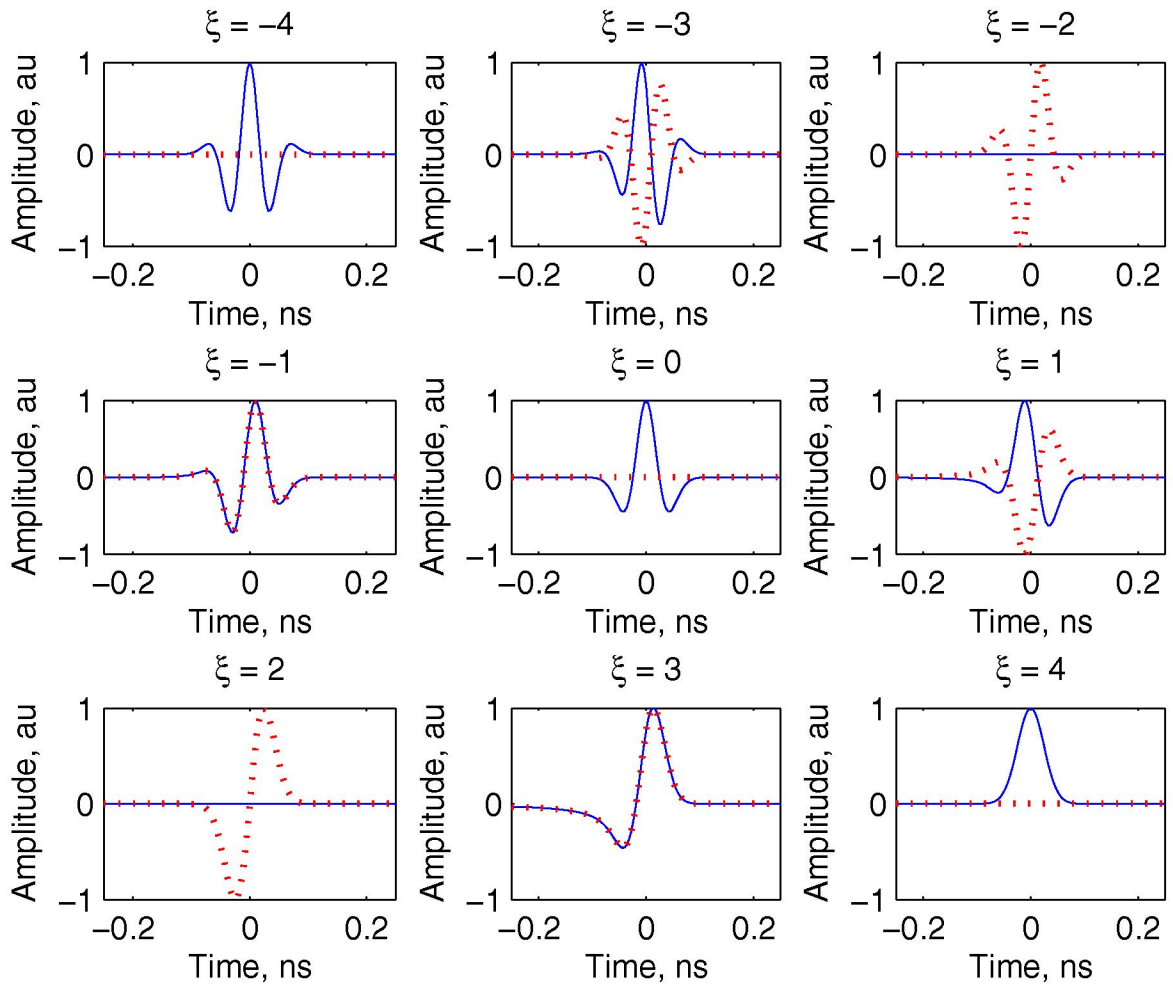

Fig. 5. Pulse distortion as a function of dispersion index, ξ. The waveforms represent the signal at the output of the receiving antenna, when the input to the transmitting antenna is the second derivative of Gaussian waveform. The amplitudes are peak-normalised and expressed in arbitrary units. The solid and dotted lines show the real (in-phase) and imaginary (quadrature) components respectively

This modelling of the FDP helps evaluate the signal distortion and consequent correlation loss at the receiver, as the variation in the degree of similarity between $s(t)$ and $r(t)$ with ξ has a strong bearing on a correlator-based impulse radio receiver. A small jitter in ξ about its nominal value – which is 2 for omni-directional antennas – causes significant waveform distortion.

Pre-empting the dispersion due to antennas, the correlation template at the receiver can be designed according to $\xi = 2$. In the light of the results of the previous section, this strategy would perform well in the V_{LOS} situation for a majority of channel instantiations. In other conditions, such as with horizontally polarized transmission, there will still be a sizeable correlation loss due to a higher average ξ. Also, under all propagation conditions, the correlation loss due to the small-scale variation of ξ, reflected in its standard deviation, cannot be removed by the antenna-distortion compensating templates. Adequate compensation of channel dispersion is therefore likely to improve link performance.

VI. Conclusion

This paper has characterized the frequency-dependent attenuation in indoor ultrawideband channels in terms of the dispersion index. In contradiction with some earlier studies, its first order statistics exhibit considerable deviation from the expected value of $\xi = 2$, more so with horizontally polarized signaling. Increasing values of ξ cause time-domain waveform distortion that can impact the performance of a UWB receiver. This point has been illustrated for Gaussian signaling, and the oscillation of the waveform energy between I/Q components as a result of variation in ξ is reported. It has been shown that a variation in ξ can change the received signal from a state of very high to very low correlation with the template, or vice versa. Our measurements have shown that UWB channels can frequently encounter such a situation, and it can disrupt reliable, error-free communications. Our future work will investigate frequency-dependent pathloss compensation and distortion mitigation strategies.

This full text paper was peer reviewed at the direction of IEEE Communications Society subject matter experts for publication in the IEEE ICC 2006 proceedings.

REFERENCES

[1] B. Allen, M. Dohler, E. E. Okon, W. Q. Malik, A. K. Brown, and D. J. Edwards, (eds.), *Ultra Wideband: Antennas and Propagation for Communications, Radar and Imaging*. London, UK: Wiley, 2006.

[2] H. Hashemi, "The indoor radio propagation channel," *Proc. IEEE*, vol. 81, July 1993.

[3] W. Q. Malik, D. J. Edwards, and C. J. Stevens, "Angular-spectral antenna effects in ultra-wideband communications links," *IEE Proc.-Commun.*, vol. 153, Feb. 2006.

[4] J. D. Kraus, *Antennas*, 2nd ed. New York, USA: McGraw-Hill, 1988.

[5] R. M. Buehrer, W. A. Davis, A. Safaai-Jazi, and D. Sweeney, "Characterization of the ultra-wideband channel," in *Proc. IEEE Conf. Ultra-Wideband Sys. Tech.* Oulu, Finland, Nov. 2003.

[6] R. C. Qiu, "A generalized time domain multipath channel and its applications in ultra-wideband (UWB) wireless optimal receiver design - part II: physics-based system design," *IEEE Trans. Wireless Commun.*, vol. 3, Nov. 2004.

[7] T. S. Rappaport, *Wireless Communications: Principles and Practice*, 2nd ed: Prentice Hall, Dec. 2001.

[8] A. Muqaibel, A. Jazi, A. Bayram, and S. Riad, "Ultra wideband material characterization for indoor propagation," in *Proc. IEEE Ant. Propagat. Soc. Int. Symp.* Columbus, OH, USA, June 2003.

[9] L. M. Frazier, "Radar surveillance through solid materials," *Proc. SPIE*, vol. 2938, 1997.

[10] R. J.-M. Cramer, R. A. Scholtz, and M. Z. Win, "Evaluation of an ultra-wide-band propagation channel," *IEEE Trans. Antennas Propagat.*, vol. 50, May 2002.

[11] W. Q. Malik, D. J. Edwards, and C. J. Stevens, "Optimal system design considerations for the ultra-wideband multipath channel," in *Proc. IEEE Veh. Technol. Conf.* Dallas, TX, USA, Sep. 2005.

[12] W. Q. Malik, D. J. Edwards, and C. J. Stevens, "Frequency dependence of fading statistics for ultrawideband systems," *IEEE Trans. Wireless Commun.*, (in press).

[13] W. Q. Malik, "Cognitive techniques for ultrawideband communications," in *Proc. IEE Sem. Ultrawideband.* London, UK, Apr. 2006.

[14] A. Alvarez, G. Valera, M. Lobeira, R. P. Torres, and J. L. Garcia, "New channel impulse response model for UWB indoor system simulations," in *Proc. IEEE Veh. Technol. Conf.* Jeju, South Korea, Apr. 2003.

[15] J. Kunisch and J. Pamp, "Measurement results and modeling aspects for the UWB radio channel," in *Proc. IEEE Conf. Ultra-Wideband Sys. Tech.* Baltimore, MD, USA, May 2002.

[16] A. F. Molisch, *et al.*, "IEEE 802.15.4a channel model - final report," IEEE 802.15-04-0662-02-004a, 2005.

[17] P. Kyritsi, D. C. Cox, R. A. Valenzuela, and P. W. Wolniansky, "Effect of antenna polarization on the capacity of a multiple element system in an indoor environment," *IEEE J. Select. Areas Commun.*, vol. 20, August 2002.

[18] K. B. Oldham and J. Spanier, *The Fractional Calculus*. New York, USA: Academic Press, 1974.

[19] M. Z. Win and R. A. Scholtz, "Impulse radio: how it works," *IEEE Commun. Lett.*, vol. 2, Feb. 1998.

This full text paper was peer reviewed at the direction of IEEE Communications Society subject matter experts for publication in the IEEE ICC 2006 proceedings.